Evoking prescribed spike times in stochastic neurons

Jens Doose and Benjamin Lindner

Bernstein Center for Computational Neuroscience, Berlin 10115, Germany
and Physics Department of the Humboldt University Berlin, Berlin 12489, Germany

Single cell stimulation *in vivo* is a powerful tool to investigate the properties of single neurons and their functionality in neural networks. We present a method to determine a cell-specific stimulus that reliably evokes a prescribed spike train with high temporal precision of action potentials. We test the performance of this stimulus in simulations for two different stochastic neuron models. For a broad range of parameters and a neuron firing with intermediate firing rates (20–40 Hz) the reliability in evoking the prescribed spike train is close to its theoretical maximum that is mainly determined by the level of intrinsic noise.

I. INTRODUCTION

The information transfer that is necessary for the perception and the complex behavior of animals is mediated by excitable neurons, the basic unit of information processing in the nervous system. It is likely that this transmission of information does not only rely on the mean activity of populations of neurons, but in some situations depends on the precise timing of action potentials (APs) of the individual neurons [1,2]. How important AP timing is compared to simple population (or rate) coding has been debated since the 1990s [3–5] but must be still regarded as an open problem (see, e.g., [6–8] for more recent contributions to the topic).

The importance of single spikes has been underlined over the past decade in a series of experiments that have shown that a few spikes evoked in single cortical neurons may affect the animals' behavior or brain state [9–12]; for a recent theoretical approach for this problem, see [13]. In these "reverse physiology" experiments the control about the neuronal dynamic is a limiting factor to further investigate the role of single neurons and AP timing. Thus new experimental methods that provide the ability to reliably manipulate the firing of individual neurons *in vivo* are needed to gain deeper insights into the role of AP timing of single neurons. In a recent publication by Doose *et al.* [14] it was shown that for individual neurons from rat sensory and motor cortex the timing of APs could be reliably controlled by juxtacellular stimulation with fluctuating Gaussian currents (frozen noise). Using the neuron's linear response function, stimuli could be computed that evoked a previously defined spike train with high reliability and temporal precision (see Fig. 1 for examples studied here in this paper).

In the present work, we explore this method in more detail using two computational models. We recall that certain constraints arising from experimental issues are characteristic for the method: We want to find a stimulus evoking a prescribed spike train under the following conditions: (1) The stimulus has a finite cutoff-frequency f_c. (2) The stimulus has Gaussian statistics with a prescribed mean μ and variance σ^2.

The limitation to a hard cutoff frequency (zero power for $f > f_c$) is needed to enable spike detection under juxtacellular current stimulation [14]: in the recorded voltage trace the noisy input signal and the spikes of the cell are superposed and the comparatively small spikes can be only extracted by filtering—which requires that the stimulus does not have any power in the high frequency band that is characteristic for the spike shape (typically for $f > 100$ Hz). The constraint of a Gaussian statistics with mean μ and variance σ^2 is motivated by the observation that these stimuli are well tolerated by the cells and that their statistics is similar to the natural input statistics of superpositions of many input spike trains. Both constraints prevent the obvious (unconstrained) solution of our problem, namely, to drive the cell with a sequence of strong excitatory input spikes positioned at the prescribed spiking times. The latter method is not unreasonable and has recently been shown to work in cortical cells [15].

Note that our objective is very different from that of approaches that mainly aim at the determination of stimulus parameters to reproduce certain interspike-interval (ISI) statistics in stochastic neuron models (reviewed in Ref. [16]). There, the neural dynamics is assumed to be subject to white-noise input for which the parameters (mean and noise intensity) are estimated. In contrast to these approaches, we do not aim at reproducing ISI statistics but want to estimate a stimulus that evokes exact spike times. To this end, we allow the input stimulus to have temporal correlations, i.e., we deal with a so-called colored noise [17].

It is plausible that the procedure works if the prescribed spike train has a similar spike statistics as a spike train of this neuron under a white-Gaussian-noise stimulus. This was the scenario that was studied in Ref. [14]. However, it is less clear if the procedure can still function if we require deviations in mean activity (firing rate) and variability (quantified by the coefficient of variation [C_V] of the interspike interval) from this reference firing statistics. Here, we extend the approach developed in Ref. [14] to evoke spike trains that can vary in their mean firing rate r and C_V over a physiologically relevant interval (see also Fig. 1 for a first impression that this method works for different parameter choices). We study this for the two-compartment model used in Ref. [14] and for a one-compartment model with parameters estimated from experiments on cortical cells [18].

In the following we first introduce the neuron models and recall basic statistic quantities that are used in this work. We then propose how we define the prescribed spike train and explain the computational method for the stimulus generation. Finally, we systematically compare prescribed and evoked spike-train statistics and analyze the generated stimuli in terms
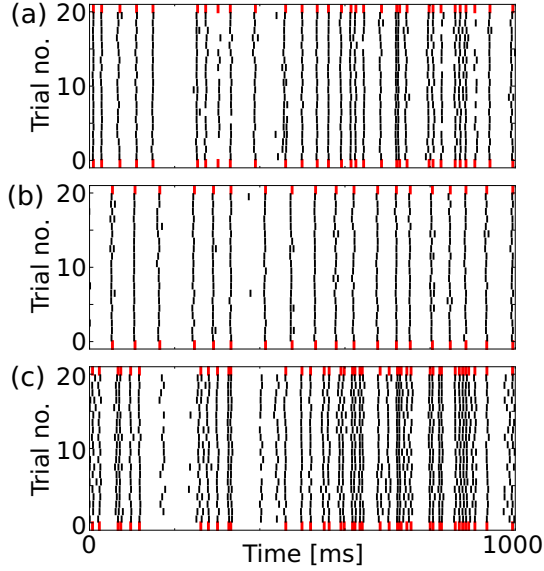
FIG. 1. Three raster plots are given for different values of the prescribed rate $r_\dagger$ and coefficient of variation $C_{V\dagger}$. The prescribed spike times are marked above and below the respective raster plot (thick, red). The upper panel shows the raster plot for reference statistics $r_\dagger = 32.7$ Hz $= r_0$ and $C_{V\dagger} = 0.68 = C_V^0$, yielding a coincidence between evoked and prescribed spike trains of $\Gamma_{sd} = 0.66$ [for this measure of similarity of spike trains, see Eq. (24)]. The middle panel is for $r_\dagger = 19.6$ Hz $< r_0$ and $C_{V\dagger} = 0.24 < C_V^0$ and yields $\Gamma_{sd} = 0.62$. The lowest panel is for increased $r_\dagger = 45.8$ Hz $> r_0$ and increased $C_{V\dagger} = 1.15 > C_V^0$ and has $\Gamma_{sd} = 0.55$.

of their power spectra. We conclude with a short summary of our results and an outlook for future extensions of the method.

II. MODELS AND METHODS

We first describe the two neuron models studied in this paper, recall then some spike-train statistics, and introduce finally different stimuli and methods to generate spike trains with prescribed statistics.

A. Neuron models

Many neural network studies employ one-compartment models and thus it is vital to understand to which extent spike timing can be controlled by a time-dependent stimulus in this model class. However, there are situations in which a one-compartment model is insufficient to reproduce quantitatively the spike statistics of a neuron and in these situations at least a two-compartment model is required [14,19]. Thus, in the following we will inspect how well spike trains can be evoked in one- and two-compartment models.

The one-compartment model is an exponential integrate-and-fire (EIF) model [20], characterized by the evolution of a single space-independent voltage variable, that describes the dynamic of an effective spike-trigger zone which is usually referred to as somatic voltage $V_s(t)$:

$$C_s \frac{dV_s}{dt} = -g_s V_s + g_s \Delta_T e^{(V_s - V_{Th})/\Delta_T} + I_{in,s} \quad (1)$$

(for the fire-and-reset mechanism, see below). For this model we used parameter values given by Harrison *et al.* [18] for pyramidal neurons from layer 2/3 of the rat somatosensory cortex (see Table 2 in Ref. [18]).

The two-compartment model consists of two coupled compartments that represent the soma and the dendrite, respectively, and its parameters are taken from fits to a pyramidal neuron in rat motor cortex [14]. The model is similar to the one used in Ref. [19] to describe the high-frequency response of Purkinje cells. As for the one-compartment model the somatic compartment (V_s) is equipped with an active spiking mechanism, while the dendritic compartment (V_d) acts purely passive. The voltage dynamic of the two-compartment model is given by

$$C_s \frac{dV_s}{dt} = -g_s V_s - g_c(V_s - V_d) + g_s \Delta_T e^{(V_s - V_{Th})/\Delta_T} + I_{in,s},$$

$$C_d \frac{dV_d}{dt} = -g_d V_d + g_c(V_s - V_d) + I_{in,d}. \quad (2)$$

In these equations C_s (C_d) is the total capacitance of the respective compartment, g_s and g_d are the somatic and dendritic leak conductance and g_c accounts for the electric coupling between both compartments, Δ_T is the spike-slope factor that defines the sharpness of the spike onset, V_{Th} is the soft threshold which has to be overcome by V_s to generate an exponential upstroke (AP). The current that enters the compartments is given by $I_{in,s} = s(t) + \sqrt{2D_s}\xi_s(t)$ for the somatic and $I_{in,d} = \mu_d + \sqrt{2D_d}\xi_d(t)$ for the dendritic compartment. Here $\xi_{s,d}(t)$ are independent white Gaussian noise processes with zero mean and unit variance that are scaled by the noise intensities D_s and D_d. Together with the constant μ_d these noise terms are supposed to account for the input of the surrounding network and cause the intrinsic variability. The stimulation current enters the dynamic in the somatic compartment and is denoted by $s(t)$. The dynamic in the somatic compartment [first equation in Eq. (2)] is completed by the fire-and-reset rule: Whenever $V_s > 6\,V_{Th}$, we set $V_s = 6\,V_{Th}$, register a spike time, and perform a reset in the somatic compartment $V_s \rightarrow 0$ in the next time step. The dendritic voltage during an action potential is only affected due to the electrotonic coupling to the somatic compartment; no reset or afterhyperpolarization is taken into account.

Both models are simulated with a stochastic Euler scheme with a time step of $dt = 0.2$ ms for a time window of $T_W = 10$ s.

B. Spike-train statistics

The spike times t_i generated by the models define the corresponding spike trains:

$$x(t) = \sum_{i=1}^{N} \delta(t - t_i). \quad (3)$$

In this paper, we consider the stationary firing rate, obtained by an average of the spike train and over stimuli

$$r = \langle x(t) \rangle, \quad (4)$$

which is a simple measure for the intensity of spiking. The coefficient of variation (CV) can be defined based on the

interspike intervals (ISIs), $T_i = t_i - t_{i-1}$,

$$C_V = \frac{\sqrt{\langle (T_i - \langle T_i \rangle)^2 \rangle}}{\langle T_i \rangle}, \tag{5}$$

i.e., the relative standard deviation of the ISI, that attains values of zero for a perfectly regular spike sequence and one for a Poisson point process.

The spectral measures studied here are all defined in terms of the Fourier transform of a general time series $x(t)$ (here not necessarily a spike train) and denoted by

$$\tilde{x}(f) = \int_0^T e^{2\pi i f t} x(t) \, dt. \tag{6}$$

In terms of the ensemble average $\langle \cdot \rangle$ and the time window T, the power spectrum is defined by

$$S_{xx}(f) = \frac{1}{T} \langle \tilde{x}^* \tilde{x} \rangle, \tag{7}$$

where * denotes complex conjugation. In the following we omit the usual limit $T \to \infty$ of the precise mathematical definition and assume that the time window $T_W = 10$ s is sufficiently large to resolve all spectral features of the process.

Equivalently, the cross spectrum between two time series $x(t)$ and $y(t)$ is given by

$$S_{xy}(f) = \frac{1}{T} \langle \tilde{x}^* \tilde{y} \rangle. \tag{8}$$

For all spike train statistics shown in this paper, we use at least 150 realizations of the stimulus and for each stimulus 20 realizations of the intrinsic noise sources, such that the ensemble comprises at least 3000 realizations in total.

C. White-noise stimuli

The stimulation current $s(t)$ is injected in the somatic compartment and different choices for its statistics are possible. Often in experiments, a white bandpass-limited Gaussian noise with sharp cutoff frequency f_c, mean μ_0, and variance σ_0^2, is used:

$$s_0(t) = \mu_0 + \sigma_0 \eta(t). \tag{9}$$

Here $\eta(t)$ is a mean-zero Gaussian noise with uniform spectral density for $f < f_c$ and a unit variance. Stimulating the neuron models by a stimulus as in Eq. (9) will give us *reference* values of rate and CV, r_0 and $C_{V,0}$, that can be achieved with Gaussian noise with this mean value and variance.

We furthermore use the white-noise stimulus to estimate two other important statistical measures: (i) the firing-rate-vs-input current relation,

$$r_0 = f_\mu(\mu_0, \sigma_0^2), \tag{10}$$

obtained by measuring the firing rate for a whole range of values of μ_0 (with a fixed σ_0^2); (ii) the dynamical susceptibility at our reference point (μ_0, σ_0^2) computed from the input-output cross spectrum $S_{s_0 x}(f)$,

$$\chi_0(f) = \frac{S_{s_0 x}(f)}{S_{s_0 s_0}(f)}. \tag{11}$$

Our parameter reference points in the following are $\mu_0 = \sigma_0 = 300$ nA for the one-compartment model [Eq. (1)] in

the suprathreshold regime, $\mu_0 = 200$ nA and $\sigma_0 = 300$ nA in the subthreshold regime and and $\mu_0 = \sigma_0 = 6000$ nA for the two-compartment model [Eq. (2)] also in the suprathreshold regime.

D. Prescribed spike trains

The main focus here is not on the white-noise stimuli as defined above but on Gaussian stimuli $s_\dagger(t)$ that are designed to evoke prescribed spike trains $x_\dagger(t)$. Before we come to the problem of how to construct these stimuli, we discuss briefly how to construct prescribed spike trains.

There are different algorithms to generate spike trains with prescribed statistics (see, e.g., [21–23]). Here we choose a simple renewal spike train with an ISI distribution following an inverse Gaussian. This distribution is completely determined by only two parameters that we can prescribe: the firing rate $r_\dagger$, characterizing the intensity of spiking, and the CV $C_{V\dagger}$, quantifying the variability of firing.

In order to generate this renewal process, one could start at a random initial time and draw subsequent ISIs from the inverse Gaussian ISI distribution with the prescribed mean and variance (determined by firing rate and CV). There is, however, a simpler alternative method: it is known that a perfect integrate-and-fire model driven by white Gaussian noise generates exactly an inverse Gaussian ISI sequence [24,25]. We choose this latter method to generate $x_\dagger(t)$ by simulating this model,

$$\frac{dV}{dt} = \alpha + \sqrt{2D}\xi(t), \tag{12}$$

where $\xi(t)$ is white Gaussian noise with $\langle \xi \rangle = 0$ and $\langle \xi(t)\xi(t') \rangle = \delta(t - t')$ and the fire-and-reset rule that whenever $V > 1$, we register a spike time and reset $V \to 0$. Given prescribed values of rate $r_\dagger$ and CV $C_{V\dagger}$, the input parameters of the model α and D are uniquely determined and read [26]

$$\alpha = r_\dagger, \quad D = \frac{r_\dagger C_{V\dagger}^2}{2}. \tag{13}$$

Turning back to the original models [Eqs. (1) and (2)], we can ask what kind of ISI statistics these models can generate. By changing the stimulus statistics within our constraints, we can certainly achieve different values of rate and CV. If we use the simple bandpass-limited white Gaussian noise with a sharp cutoff frequency, Eq. (9), we obtain the aforementioned reference values of rate and CV, r_0 and $C_{V,0}$. It is clear, that it will not be difficult to obtain similar values if we use a more general kind of stimulus. One of our main questions here, though, is to which extent spike trains can be evoked that deviate in their statistics from r_0 and $C_{V,0}$.

E. Stimuli that evoke prescribed spike trains

In the following we outline how a Gaussian noise with sharp cutoff frequency can be estimated that will (approximately) evoke the prescribed spike train in the neuron model under investigation (for a sketch of the procedure, see Fig. 2). The main difference of this stimulus class to our reference stimulus $s_0(t)$ is that the power spectrum of $s_\dagger(t)$ is not uniform but can have an arbitrary shape in the range $(0, f_c)$ (fluctuations with
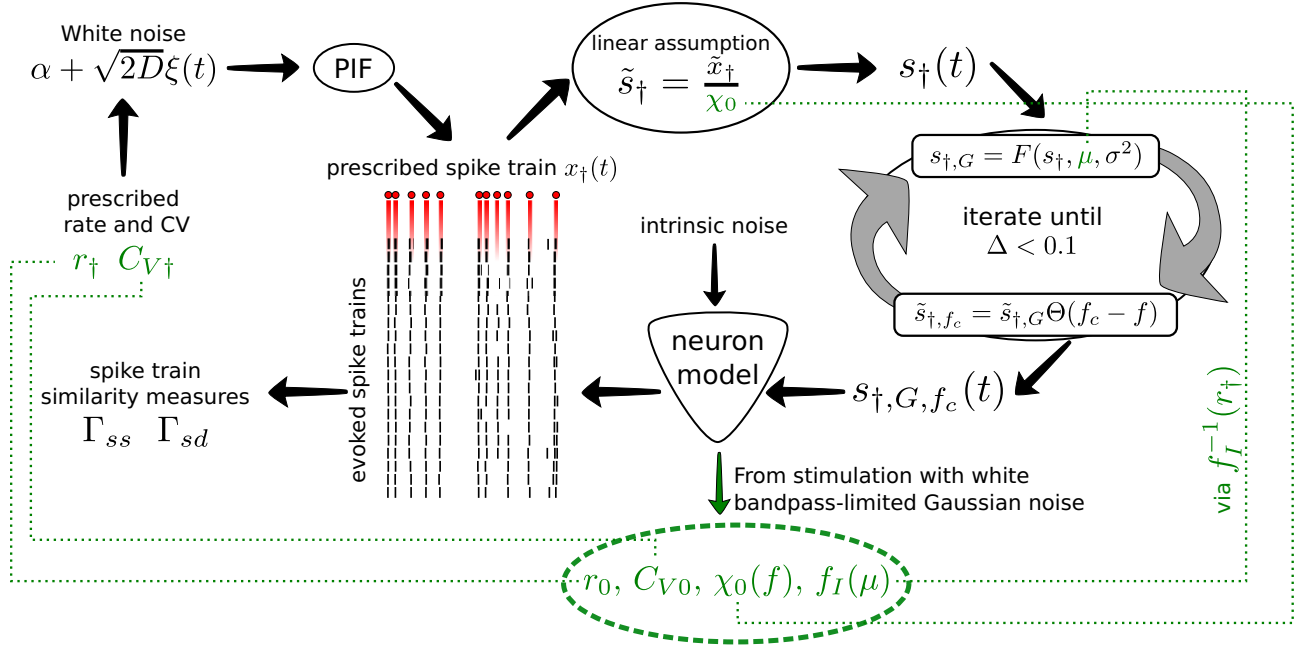
FIG. 2. Schematic representation of the procedure that generates prescribed spike trains by simulating a (one- or two-compartment) neuron model with colored Gaussian noise with a given cutoff frequency f_c. The green (dotted) lines indicate which parts of the procedure are influenced by model-specific properties (listed in the dashed ellipse). For a pseudo code of the procedure, see Sec. II F.

a nonflat power spectrum are generally referred to as *colored noise* [17]).

For a linear system output $x(t)$ and input $s(t)$ are related via

$$x(t) = K * s(t). \qquad (14)$$

Here $K(t)$ is the linear response function that completely defines the system and $*$ denotes convolution. In the frequency domain the convolution simplifies to a multiplication

$$\tilde{x}(f) = \chi(f)\tilde{s}(f), \qquad (15)$$

where the Fourier-transform of $K(t)$ is the susceptibility $\chi(f)$. This linear description must be regarded as a rough approximation of the full system because the neuron converts a continuous input signal into a series of action potentials (a point process) and therefore acts highly nonlinearly.

In the following we use exclusively the susceptibility $\chi_0(f)$ from Eq. (11) measured with white-noise stimuli at the respective reference point μ_0, σ_0^2. Besides the assumed linearity, this constitutes another approximation because the susceptibility depends both on μ_0 and σ_0^2 as well as on the color of the noise (for a simple example of the latter dependence, see [20]). With the knowledge of the susceptibility we can use Eq. (15) to calculate the stimulus $\tilde{s}_\dagger(f)$ that evokes the output $\tilde{x}_\dagger(f)$:

$$\tilde{s}_\dagger(f) = \frac{\tilde{x}_\dagger(f)}{\chi_0(f)}, \qquad (16)$$

and use the inverse Fourier transform to determine the corresponding time series $s_\dagger(t)$. However, $s_\dagger(t)$ does in general not satisfy our constraints: (i) a certain variance and mean, (ii) Gaussianity, and (iii) a sharp cutoff frequency f_c. To impose these restrictions, we proceed as follows.

In a first step we apply a static nonlinearity $F(s)$ to the stimulus in the time domain:

$$s_{\dagger,G}(t) = F(s_\dagger(t),\mu,\sigma^2). \qquad (17)$$

We choose the nonlinearity F such that the transformed stimulus possesses Gaussian statistics with mean value μ and variance σ^2 (for how μ and σ^2 are specified, see below). The nonlinearity F can be expressed by the cumulative probability density of the actual stimulus $P_\dagger$ and the inverse cumulative probability distribution of a Gaussian signal P_G^{-1} (the inverse of the prescribed probability distribution):

$$F(x,\mu,\sigma^2) = P_G^{-1}(P_\dagger(x),\mu,\sigma^2). \qquad (18)$$

Although the stimulus $s_{\dagger,G}(t)$ is Gaussian, it does not obey the constraint of a sharp cutoff frequency. This can be achieved by Fourier transformation of $s_{\dagger,G}(t)$, setting all Fourier-components above f_c to zero,

$$\tilde{s}_{\dagger,f_c}(f) = \tilde{s}_{\dagger,G}(f)\Theta(f_c - f), \qquad (19)$$

and, subsequently, transforming $\tilde{s}_{\dagger,f_c}(f)$ back to the time domain. This second (temporal) transformation can change the stimulus' statistics to having a non-Gaussian probability density again. To obtain a stimulus that fulfills all constraints at the same time, we iteratively apply Eqs. (17) and (19) (for similar iterative schemes, see [27]).

To quantify the convergence of the iterative process we define a measure for the similarity between two cumulative probability distributions:

$$\Delta = \frac{\int_{-\infty}^{\infty} \left| P_{\dagger,f_c}(s) - P_G(s) \right| ds}{\int_{-\infty}^{\infty} |P_{G'}(s) - P_G(s)| ds}. \qquad (20)$$

Here $P_G(s)$ and $P_{G'}(s)$ are cumulative probability distributions of two Gaussian variables that have the same mean value but

slightly different standard deviations σ and $\sigma' = 1.01\sigma$. Thus, the difference between these distributions (denominator) is used as a reference value for the difference between the actual probability distribution and the prescribed one (numerator). We use $\Delta < 0.1$ as the termination criterion for the iteration, i.e., the cumulative distribution of $s_{\dagger,G,f_c}(t)$ should differ from the associated Gaussian by less than 10% of what would be the deviation between two Gaussians that differ in their standard deviations by 1% . Typically after 10–20 iterations this criterion is fulfilled and the procedure provides a stimulus $s_{\dagger,G,f_c}(t)$ that satisfies approximately all constraints. In the following, we will write $s_\dagger(t)$ instead of $s_{\dagger,G,f_c}(t)$ to ease the notation.

How should we choose μ and σ^2 in Eq. (17)? As an experimental constraint we adopt a fixed value of the stimulus variance $\sigma^2 = \sigma_0^2$ because the total power injected in the cell should be limited (these values need to be tolerated by the cell without causing damage). Because the firing rate depends strongly on the mean input current, we do not keep the mean value μ fixed but let it depend on the prescribed firing rate $r_\dagger$ via the inverse firing-rate-vs-input-current relation for the white-noise driven IF model, i.e., the inverse of Eq. (10):

$$\mu = f_\mu^{-1}(r_\dagger). \tag{21}$$

This is certainly an approximation because $s_\dagger(t)$ is not a bandpass-limited white but a colored Gaussian noise and the noise color can affect the firing rate [28]. However, as we will see below, the deviations due to this approximations are small.

F. Pseudoalgorithm

For a better understanding of the procedure, in the following we present a pseudoalgorithm that illustrates the computation of the stimulus $s_\dagger(t)$.

---

procedure CALCULATE STIMULUS
    define neuron model   ▷ Eqs. (1), (2)
    set μ_0 and σ_0 to suitable values
    ▷ determination of the reference statistics
    for η in reasonable set of realizations **do**
        $s_0(t) = \mu_0 + \sigma_0\eta(t)$ ▷ Eq. (9)
        stimulate neuron with $s_0(t)$
        measure output spike trains
        estimate $r_0, C_{V,0}, \chi_0(f)$ ▷ Eqs. (4), (5), (11)
    end for
    ▷ estimate firing-rate vs input-current relation
    for μ in plausible range around μ_0 **do**
        for s_0 in reasonable set of realizations **do**
            stimulate neuron with $s_0(t) - \mu_0 + \mu$
            measure output firing-rate $f_\mu(\mu,\sigma^2)$
        end for
    end for
    set $r_\dagger$ and $C_{V\dagger}$ in a range around r_0 and $C_{V,0}$
    $\alpha = r_\dagger$ ▷ Eq. (13)
    $D = \frac{r_\dagger C_{V\dagger}^2}{2}$ ▷ Eq. (13)
    stimulate PIF with $\alpha + \sqrt{2D}\xi(t)$ ▷ Eq. (12)

    $\to x_\dagger(t)$
    $\tilde{x}_\dagger(f) = \mathcal{F}(x_\dagger)$ ▷ Fourier transform
    $\tilde{s}_\dagger(f) = \tilde{x}_\dagger/\chi_0$ ▷ Eq. (16)
    $s_\dagger(t) = \mathcal{F}^{-1}(\tilde{s}_\dagger(f))$ ▷ Inverse Fourier transform
    $\mu_\dagger = f_\mu^{-1}(r_\dagger,\sigma_0)$ ▷ Eq. (21)
    while $\Delta > 0.1$ **do**
        $s_\dagger(t) \to P_\dagger(s_\dagger)$ ▷ estimating cumulative prob.
        $s_{\dagger,G} = P_G^{-1}(P_\dagger(s_\dagger(t)),\mu_\dagger,\sigma_0^2)$ ▷ Eq. (17)
        $\tilde{s}_{\dagger,f_c}(f) = \mathcal{F}(s_{\dagger,G}(t))\Theta(f_c - f)$ ▷ Eq. (19)
        $s_\dagger(t) = \mathcal{F}^{-1}(\tilde{s}_{\dagger,f_c}(f))$
        calculate $\Delta(s_\dagger(t))$ ▷ Eq. (20)
    end while
    return $s_\dagger(t)$
end procedure

G. Measures of spike-train similarity

Because a coarse approximation [Eq. (14)] and some *ad hoc* transformations [Eqs. (17) and (19)] are used to calculate our stimulus $s_\dagger(t)$, we need to test the performance of the computed stimulus to evoke the prescribed spike train $x_\dagger(t)$. To this end, we use a coincidence measure that defines the similarity between two spike trains a and b with counts N_a and N_b within a time window T as [29]

$$\Gamma_{a,b} = \frac{1}{1 - 2\Delta N_a/T}\frac{N_{\text{coin}} - N_{\text{chance}}}{\frac{1}{2}(N_a + N_b)}. \tag{22}$$

In this formula the count of coincident spikes (determined with a temporal precision of $\pm\Delta$) is referred to as N_{coin}, the chance level for two independent spike trains is given by $N_{\text{chance}} = 2\Delta N_a N_b/T$, and the normalization prefactor in Eq. (22) ensures that $\Gamma_{a,b}$ is bound by 1. Specifically, $\Gamma_{a,b}$ is 0 for independent and is 1 for identical spike trains, respectively. Throughout, we will use $\Delta = 2.5$ ms as the temporal precision for coincident spikes.

Generally, the measure $\Gamma_{a,b}$ [Eq. (22)] is asymmetric in N_a and N_b and therefore, if the spike trains a and b have different firing rates, $\Gamma_{a,b}$ is affected by the order of a and b [30]. However, in the following we ensure that all spike trains that are compared by this measure have a similar firing rate such that this asymmetry can be neglected.

In the following we will apply the coincidence measure to two *output* spike trains that are evoked by the same stimulus,

$$\Gamma_{ss} = \langle\Gamma_{a,b}\rangle_{a\neq b}, \tag{23}$$

where the average runs over all combinations of distinct spike trains, labeled by indices a and b [all supposed to evoke the same prescribed spike train $x_\dagger(t)$] and over all stimulus realizations. We can, however, also ask how similar the output spike train $x(t)$, labeled by the index a, is to the prescribed spike train $x_\dagger(t)$, labeled by the index d, which is quantified by

$$\Gamma_{sd} = \langle\Gamma_{a,d}\rangle_{a,d}. \tag{24}$$

Here the second spike train (d) is simply $x_\dagger(t)$ and we average over all spike trains a that are evoked by the prescribed stimulus $s_\dagger(t)$ [which has been computed from $x_\dagger(t)$]and over all different realizations of prescribed spike trains d.

In summary, Γ_{ss} quantifies the intrinsic reliability of a simulated dataset while Γ_{sd} measures the similarity between simulated and prescribed spike trains.

III. RESULTS

The method described above can be applied to a real neuron (as was done in Ref. [14]) or to neuron models of varying complexity. Here we want to test the method with the two neuron models given in Eqs. (1) and (2). For the one-compartment model we make the distinction between the suprathreshold and subthreshold regime, while results for the two-compartment model are only given for the suprathreshold regime. We choose these two models because they have been used to describe the statistics of distinct cell types and because they differ in their complexity and also in their susceptibility. Hence, the comparison of the method's performance for the two models should give us an impression of its robustness. In particular the difference in the susceptibility (an important model characteristics) is remarkable: while the one-compartment model shows a monotonic decrease with frequency in our specific parameter setting and can in general also show resonances at intermediate frequencies (see, e.g., [20,31]), the susceptibility of the two-compartment model can increase monotonically with frequency [14,19].

A. Results for the one-compartment model

When attempting to evoke spike trains with specific statistics, it is plausible that the success depends on the similarity between the statistics we try to evoke and the reference statistics of the neuron under white-noise stimulation. It may also depend on in which firing regime (either suprathreshold, i.e., mean driven, or subthreshold, i.e., fluctuation driven) the stimulated cell operates. In the following, we study systematically the performance of the method, first for the suprathreshold and then for the subthreshold regimes.

Suprathreshold regime. In Fig. 1 three raster plots illustrate the model response to the calculated stimulus for prescribed spike trains $x_{\dagger}(t)$ (shown by red, thick markers above and below the trials) of different intensity and variability.

For the top raster plot [Fig. 1(a)] the prescribed spike train statistics agrees with the reference statistics ($r_{\dagger} = 32.7$ Hz $= r_0$, $C_{V\dagger} = 0.68 = C_{V,0}$). This is the case that has been investigated experimentally by Doose *et al.* [14]. As we can expect from this previous study, the method seems to work well and the generated spike times coincide reliably with the prescribed spike times.

Figure 1(b) displays a raster plot for which the prescribed rate and CV are lower than the reference statistics: $r_{\dagger} = 19.6$ Hz $< r_0$, $C_{V\dagger} = 0.24 < C_{V,0}$. Such a more regular spike train with a lower rate can also be reliably evoked with our scheme. This is somewhat in contrast to the opposite case of a prescribed spike train with increased rate $r_{\dagger} = 45.8$ Hz $> r_0$ and increased variability $C_{V\dagger} = 1.15 > C_{V,0}$ [Fig. 1(c)]. In this case, the evoked and the prescribed spike trains are less similar than for the other cases. In particular, the long ISIs that were present in the prescribed spike train are not reliably reproduced by the evoked spike trains.
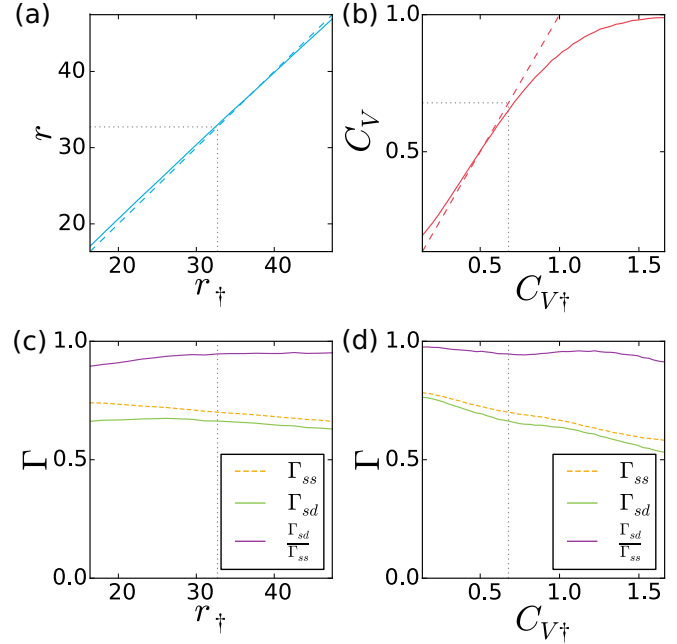

FIG. 3. One-compartment model, Eq. (1). Performance of the method in reproducing the prescribed statistics and spike times: (a) evoked rate r over the prescribed rate $r_{\dagger}$; (b) evoked C_V over the prescribed $C_{V\dagger}$; (c) intrinsic reliability, Γ_{ss} (middle, dashed curve), the similarity between evoked and prescribed spike trains, Γ_{sd} (lower curve), and the ratio of both (upper curve) as functions of the prescribed firing rate $r_{\dagger}$; (d) same as in (c) but vs prescribed $C_{V\dagger}$.

To investigate more systematically how under the imposed constraints rate and CV of the prescribed spike train can be matched by the evoked spike train, we compare in Fig. 3 the evoked rate r and C_V with the prescribed rate $r_{\dagger}$ and $C_{V\dagger}$. Deviations from the dashed diagonal lines (identity between evoked and prescribed statistics) quantify the failure in reproducing the basic statistics (dotted lines indicate the reference statistics r_0 and $C_{V,0}$). Figure 3(a) illustrates that the evoked rate successfully reproduces the prescribed rate (the resulting rate is very close to the diagonal). This is not so surprising because we use for the mean input Eq. (21), i.e., the value of μ that evokes the prescribed firing rate in an IF model with bandpass-limited white noise. Deviations could be possible because the noise is not white anymore but colored. However, the small deviations indicate that the effect of the noise color on the mean rate is minor.

The variability of firing as quantified by the CV [Fig. 3(b)] is close to the prescribed value only for values smaller or equal to $C_{V,0}$ (here the mean input and the firing rate is fixed). Apparently, by changing the color of the noise, it is possible to reduce the variability of firing but it seems to be more difficult to increase the variability (at least, with our method and compared to the case of bandpass-limited white noise). These observations are in line with our discussion of the raster plots in Fig. 1. We expect that the prescribed CV may be reproducible over the entire range if the constraint of a fixed variance σ^2 would be relaxed.

For spike trains with comparable rates it is reasonable to calculate spike train similarity in terms of the coincidence factor between output spike trains, Eq. (23), and between
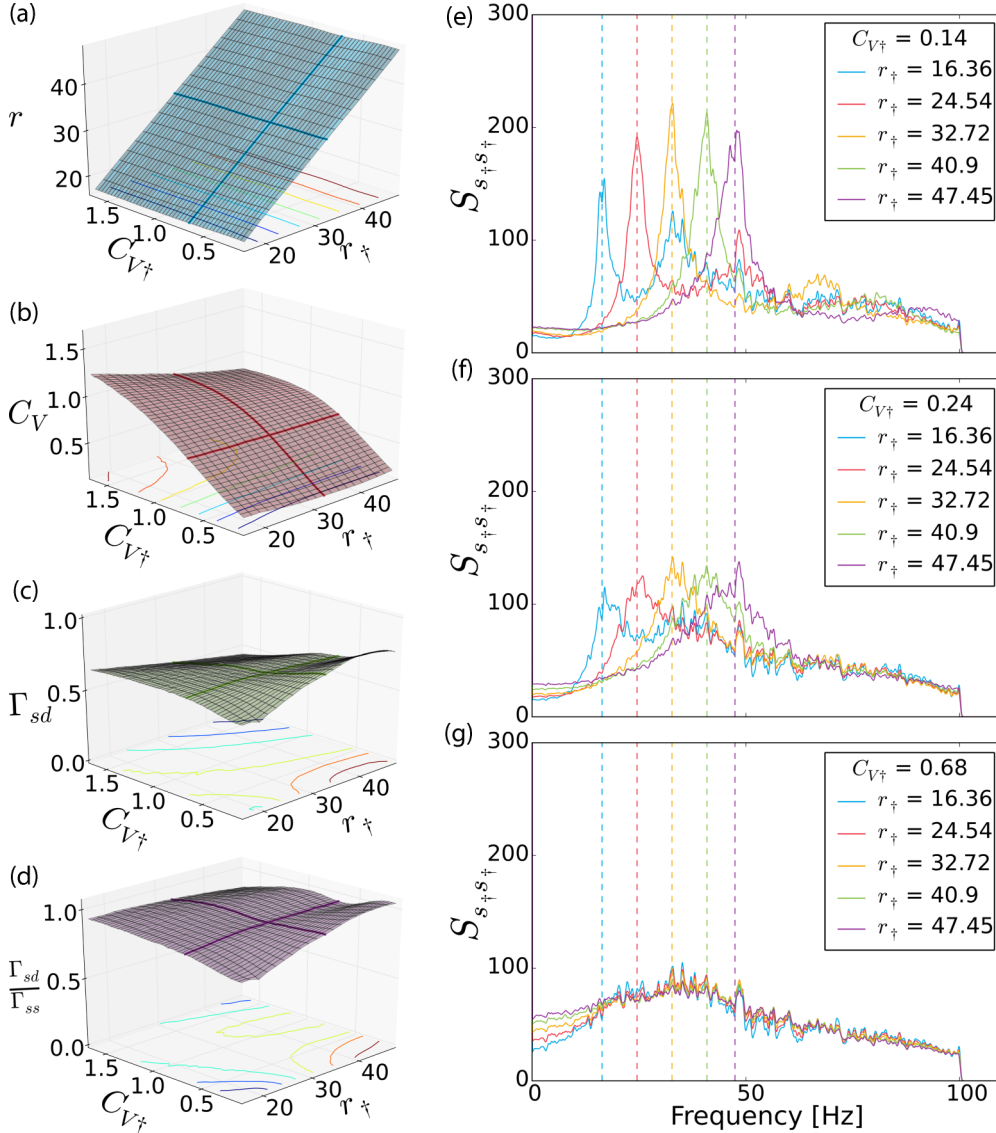
FIG. 4. One-compartment model, Eq. (1), suprathreshold (mean driven) firing regime. Comparison between prescribed and evoked rate and coefficient of variation (a),(b) and between prescribed and evoked spike times (c),(d); power spectra of designed Gaussian stimuli (e)–(g). Thick lines within the surfaces indicate either $r_\dagger = r_0$ or $C_{V\dagger} = C_{V,0}$ and the intersection corresponds to the reference statistics r_0, $C_{V,0}$ in Fig. 1(a). (a) The evoked firing rate in the plane of prescribed rate $r_\dagger$ and $C_{V\dagger}$. (b) Same as (a) but with evoked C_V on the z axis. (c) Same as (a) but with the similarity between prescribed and evoked spike trains Γ_{sd} on the z axis. (d) Same as (a) but the ratio of similarity and intrinsic reliability Γ_{sd}/Γ_{ss} on the z axis. (e)–(g) Power spectra of the evoked stimuli for different values of $r_\dagger$ and $C_{V\dagger}$ as indicated. Different rates are color-coded and marked by the vertical dashed lines at the respective frequency values; peak frequencies in (e), (f) increase with and appear close to the firing rate.

output and prescribed spike trains, Eq. (24). In Figs. 3(c) and 3(d) we show the coincidence factor between simulated spike trains Γ_{ss} (quantifying the intrinsic reliability), the similarity between simulated and prescribed spike trains Γ_{sd}, and the ratio of both coincidence factors Γ_{sd}/Γ_{ss} vs the values of the prescribed rate [Fig. 3(c)] or CV [Fig. 3(d)].

Over the whole range of firing rates [Fig. 3(c)] both measures reveal with $\Gamma_{ss} > \Gamma_{sd} > 0.6$ a large similarity between evoked and prescribed spike times. Furthermore, the two factors are almost constant and close to each other (Γ_{sd}/Γ_{ss} close to 1), i.e., the output spike trains are roughly as similar to the prescribed spike train as they are similar to each other. Hence, our method appears to work equally well

for a whole range of firing rates and we can reproduce the prescribed spike times with a high reliability.

The similarity measures display a weak dependence on the variability of the prescribed spike train $C_{V\dagger}$ [Fig. 3(d)]. As can be expected from the above considerations, the similarity is smaller for a prescribed spike train with higher variability. We note in addition that although we found in Fig. 3 that $\Gamma_{sd} < \Gamma_{ss}$, this is not the case for all parameter values (for counter examples, see below).

In Fig. 3 we have only varied one parameter of the prescribed spike train at a time, either $r_\dagger$ or $C_{V\dagger}$, while the respective other parameter was kept at its reference value. In Fig. 4 output rate and CV and the similarity measures
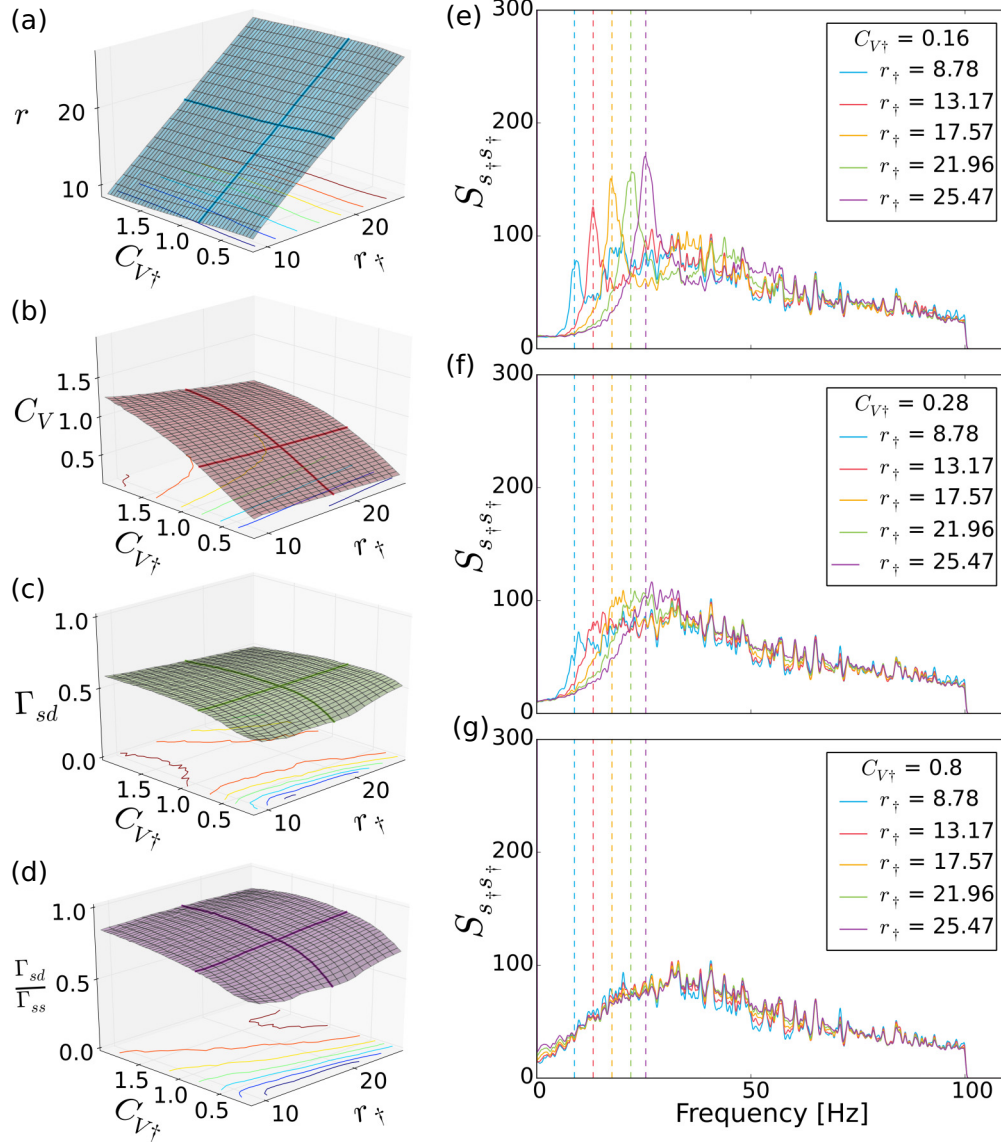
FIG. 5. One-compartment model, Eq. (1), subthreshold (fluctuations driven) firing regime. Comparison between prescribed and evoked rate and coefficient of variation (a),(b) and between prescribed and evoked spike times (c),(d); power spectra of designed Gaussian stimuli (e)–(g). Thick lines within the surfaces indicate either $r_\dagger = r_0$ or $C_{V\dagger} = C_{V,0}$ and the intersection corresponds to the reference statistics $r_0, C_{V,0}$ in Fig. 1(a). (a) The evoked firing rate in the plane of prescribed rate $r_\dagger$ and $C_{V\dagger}$. (b) Same as (a) but with evoked C_V on the z axis. (c) Same as (a) but with the similarity between prescribed and evoked spike trains Γ_{sd} on the z axis. (d) Same as (a) but the ratio of similarity and intrinsic reliability Γ_{sd}/Γ_{ss} on the z axis. (e)–(g) Power spectra of the evoked stimuli for different values of $r_\dagger$ and $C_{V\dagger}$ as indicated. Different rates are color coded and marked by the vertical dashed lines at the respective frequency values; peak frequencies in (e) increase with and appear close to the firing rate.

are shown as functions of both $r_\dagger$ and $C_{V\dagger}$, which is the result of extensive numerical simulations: at 920 parameter values we simulated 150 realizations of prescribed spike trains and applied the iterative scheme to each of those yielding in total 138 000 stimuli $s_\dagger(t)$. For each stimulus, we use then 20 realizations of the intrinsic noise to obtain the statistics of interest (output rate, CV, and similarity measures depending on the prescribed values $r_\dagger, C_{V\dagger}$).

We find that the prescribed rate is well matched by the simulations [Fig. 4(a)], independent of the prescribed $C_{V\dagger}$. The output variability [Fig. 4(b)], however, can be matched only for CVs close to or smaller than $C_{V,0}$. For larger prescribed values,

$C_{V\dagger} > C_{V,0}$ we observe distinct deviations from the prescribed values and these deviations are larger for large values of the prescribed firing rate.

In Figs. 4(c) and 4(d) the similarity between evoked and prescribed spike trains and the ratio of similarity and intrinsic reliability are plotted. The overall performance is quite good with $\Gamma_{sd} > 0.5$ for all regions in which the prescribed $C_{V\dagger}$ was successfully generated. For larger prescribed $C_{V\dagger}$ and $r_\dagger$ the similarity between evoked and prescribed spike trains decreases. The ratio of similarity and intrinsic reliability Γ_{sd}/Γ_{ss} attains values close to 1 for the whole region under investigation.

Besides the aspect of reproducing the prescribed spike trains it is also of interest to see what the statistics of the respective stimulus look like. We emphasize that this reverses the situation commonly studied, namely, how a neuron responds to stochastic stimuli of a certain statistics. In contrast, here we fix the output statistics and compute the corresponding input statistics—within the framework of the imposed constraints, of course, that imply a constant area under the power spectrum (yielding the fixed variance) and vanishing power for $f > f_c$.

In Figs. 4(e)–4(g) power spectra $S_{s_\dagger s_\dagger}(f)$ for stimuli that correspond to different prescribed rates $r_\dagger$ and $C_{V\dagger}$ are displayed. Typically, for neurons that fire more regularly (i.e., with a low CV), the power spectrum is sharply peaked around the respective firing rate [Fig. 4(e)]. With increasing CV [Figs. 4(f) and 4(g)], the stimulus power spectrum broadens and, interestingly, the power spectra for different prescribed values of the rate become more and more similar. In all panels, spectra are only shown for cases in which the prescribed CV, $C_{V,\dagger}$, could be well matched by the CV of the output spike train.

Subthreshold regime. The results for the one-compartment model in the subthreshold firing regime are shown in Fig. 5 and are similar to that for the suprathreshold regime. For these simulations the reference mean input has been reduced ($\mu_0 = 200$ nA) while all other parameters are unchanged. Lowering the mean input also changes the reference value for the firing rate and CV ($r_0 = 17.6$, $C_{V,0} = 0.8$). In Fig. 5(a), we observe that the prescribed firing rate is well reproduced in the whole range of investigated firing parameters, while the prescribed CV [Fig. 5(b)] can only be roughly matched for values smaller than $C_{V,0}$ and this discrepancy is particularly pronounced for larger values of $C_{V\dagger}$, similar to the behavior in the suprathreshold regime.

In terms of the coincidence measures [Figs. 5(c) and 5(d)], the method works reasonably well but shows decreased performance for more regular spike trains (lower $C_{V\dagger}$). The stimulus power spectra [Figs. 5(e)–5(g)] qualitatively agree with that for the suprathreshold case. For regular spiking, they show pronounced peaks around the prescribed firing rate [Figs. 5(e) and 5(f)] that are absent for larger values of $C_{V\dagger}$ [Fig. 5(g)].

At low frequencies, the stimulus power spectra are more strongly reduced than is the case in the suprathreshold regime. One reason for this is the different shape of the susceptibility (Fig. 6) that shows a more pronounced low-pass behavior for the subthreshold case. The shape of the susceptibility certainly strongly affects the power spectrum of our first guess for the correct stimulus given in Eq. (16). In particular, because in Eq. (16) we divide by χ_0, i.e., a low-pass function, we amplify the fluctuation amplitudes at higher frequencies in the stimulus; this effect is more pronounced for stronger decreasing χ_0. However, this is certainly not a strict argument, because the final stimulus, the power spectrum of which is shown in Figs. 5(e)–5(g), has the spectrum of a nonlinearly transformed variant of Eq. (16) due to the iterative steps that impose the constraints of Gaussian statistics and finite-cutoff frequency.

In summary, the one-compartment EIF model can be stimulated with a Gaussian noise to obtain a prescribed spike train with firing rate and CV that vary over the physiological range.
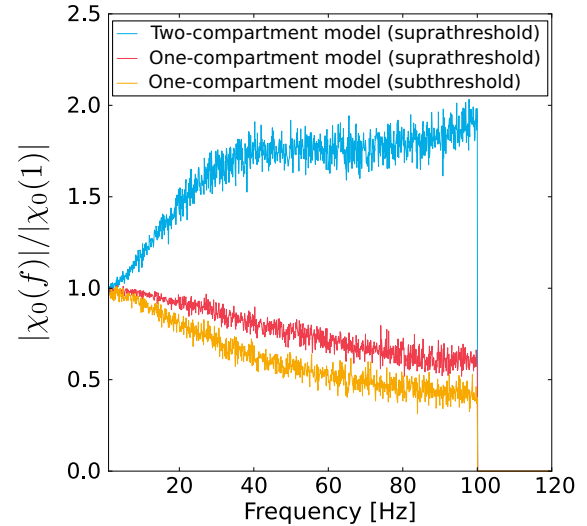

FIG. 6. Susceptibility (absolute value) of the neuron models for the cases: One-compartment model in subthreshold regime (yellow, bottom line), One-compartment model in the suprathreshold regime (red, middle line), two-compartment model in the suprathreshold regime (blue, upper line).

B. Two-compartment model

We now turn to the two-compartment model, for which the results are summarized in Fig. 7. Because (i) the neuron model possesses two compartments, (ii) the parameters of the model are quite different than for the one-compartment model, and (iii) the stimulus is stronger in this case, we find quantitative differences in all statistical measures. However, the qualitative overall appearance is not so different from the one-compartment model and reveals also for this model class a good agreement between prescribed and evoked spike trains over a broad range of parameters.

For the basic spike train statistics we obtain as in the one-compartment model that the prescribed firing rate is well matched [Fig. 7(a)] while the CV can be matched within our constraints only if it is smaller or equal to the reference value [Fig. 7(b)]. For all parameter values for which a good match in rate and CV can be achieved, we obtain also a significant similarity between prescribed spike train and output spike train [Fig. 7(c)], i.e., $\Gamma_{sd} > 0.5$. The fraction Γ_{sd}/Γ_{ss} [Fig. 7(d)] is close to 1 and in a broad parameter region even larger than 1. This means that on average the evoked spike train is more similar to the prescribed spike train than it is to a spike train evoked in another trial.

As for the one-compartment model, the power spectra of the stimuli show pronounced peaks at the prescribed firing rate for regular firing [small $C_{V\dagger}$ in Fig. 7(e)]. With increasing $C_{V\dagger}$ [Figs. 7(f) and 7(g)] these peaks broaden and vanish and the spectra become more similar for different $r_\dagger$. In contrast to the one-compartment model, the power spectra do not have a dip at low frequencies but continuously decrease with increasing frequency. This seems to be related to the shape of the susceptibility, which is high-pass for this model (see Fig. 6); this is similar to the arguments that we used when discussing the reduced low-frequency power of the stimulus for the one-compartment model in the subthreshold regime:
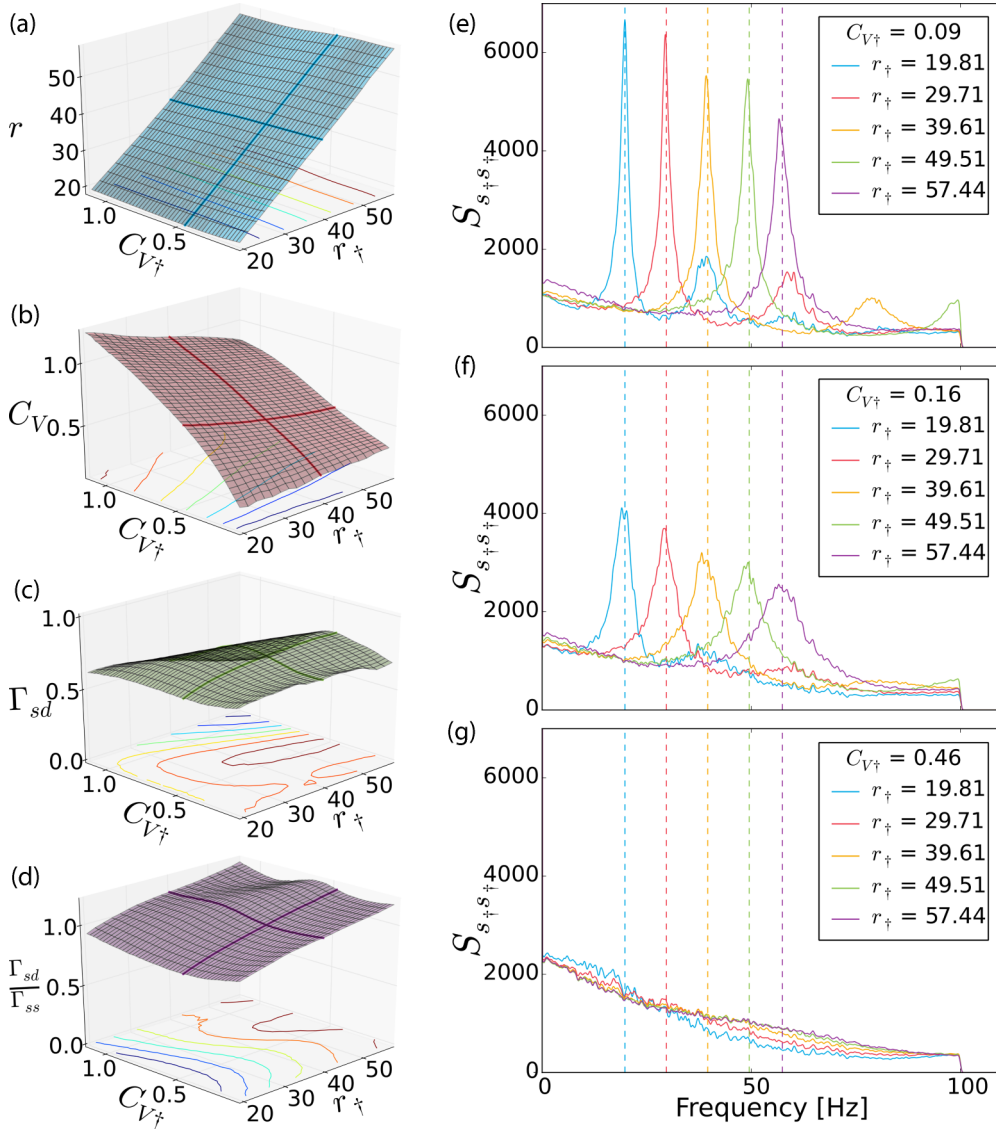
FIG. 7. The performance of the two-compartment EIF model plotted in the ($r_\dagger$, $C_{V\dagger}$) plane (a)–(d). A comparison between prescribed and evoked rate and coefficient of variation (a),(b) and between prescribed and evoked spike times (c),(d). The lines on the ground denote contour lines of equal height, the thick lines within the surfaces mark the cases where either $r_\dagger = r_0$ or $C_{V\dagger} = C_{V,0}$. (a) The evoked firing rate in the plane of prescribed rate $r_\dagger$ and $C_{V\dagger}$. (b) Same as (a) but with evoked C_V on the z axis. (c) Same as (a) but with the similarity between prescribed and evoked spike trains Γ_{sd} on the z axis. (d) Same as (a) but the ratio of similarity and intrinsic reliability Γ_{sd}/Γ_{ss} on the z axis. (e)–(g) The power spectra of the stimuli for different $r_\dagger$ and $C_{V\dagger}$. Different rates are color coded and marked by the vertical dashed lines at the respective frequency values; peak frequencies in (e), (f) increase with and appear close to the firing rate.

the division by χ_0 in Eq. (16) turns the high-pass shape of the susceptibility (Fig. 6) into a low-pass shape in the power spectrum of the stimulus [Fig. 7(g)]. Again this argument is not rigorous because after division by the susceptibility, the stimulus undergoes a number of nonlinear transformations to impose the constraints of Gaussianity and vanishing power beyond the cutoff frequency.

IV. DISCUSSION

We have tested the procedure to evoke a prescribed spike train by a correlated Gaussian stimulus with sharp cutoff frequency for two stochastic neuron models and for the sub- and suprathreshold firing regime. We extended

the original procedure developed in Ref. [14] to the case that the firing rate and the coefficient of variation deviate substantially from the typical values observed for a white-noise stimulus. Over a broad physiological range of parameters, we could design Gaussian stimuli that indeed evoked in the neuron model the prescribed spike trains with high reliability.

In our study we did not optimize the input statistics in order to match the rate and CV between prescribed and evoked spike trains. However, in most cases such a match was achieved as a by-product of our procedure of transferring the prescribed spike train into a stimulus. Thus, an interesting result of our efforts is the power spectrum of stimuli that evoke spike trains with a certain rate and CV.

For regular spiking (small $C_{V\dagger}$) the power spectrum of the driving noise has a pronounced peak at the prescribed firing rate. Hence, if we are free to distribute the noise power over frequencies (within the prescribed frequency band), fluctuations seem to be least *harmful* for the regularity of firing if the main power is distributed around the firing rate. This is an important insight that deserves further exploration: In general, it is quite difficult to predict how the shape of the noise spectrum will affect the firing statistics of a spike-generating (hence highly nonlinear) neuron model (for some analytical results on this problem for simple integrate-and-fire neurons, see [32–34]).

For more irregular spiking (larger $C_{V\dagger}$) the spectrum becomes broader and the peak vanishes. The results for the two-compartment model indicate that a particularly irregular spike train can be generated by a Gaussian noise that has most power at low frequencies. We suspect that the variability-maximizing power spectrum would be achieved for an infinitely slow stimulus (all power at zero frequency) because for such a static stimulus ensemble the single realization of the noise does not suffer any self-averaging that diminishes the ISI variability of the driven cell. Also this limit of high variability under a colored-noise driving is largely unexplored (for some exceptions, see the review [35] and references therein).

For simplicity we restricted this study to prescribed spike trains that are renewal processes. In contrast, many neurons show ISI correlations [36] and these correlations can be important for information transmission [37–39]. It is therefore an interesting question how ISI correlations in the prescribed spike train will affect our results. As shown in Ref. [34], temporal correlations in the input, i.e., the noise color, can cause negative ISI correlations. Therefore, correlations of the intervals in the prescribed spike train will presumably cause a modification of the color of the input stimulus. Hence, we expect that our method will also work for prescribed spike trains with ISI correlations.

In this study the performance of our method was demonstrated for two different neuron models (one-compartment or two-compartment EIF models) and different parameter sets, illustrating in this way the method's robustness. For both models we observed that the discrepancy between the CV of the prescribed spike train and that of the evoked spike train was largest for high CV. This inability of our method to evoke more irregular spike trains is likely due to the constraint of a constant stimulus variance. We recall that this constraint was imposed because living neurons tolerate only stimuli up to a certain input power. Note that even with a constraint stimulus variance it would presumably be possible to evoke spike trains with a high CV with neuron models that possess an intrinsic bursting mechanism [40,41].

Because our method relies on the measurements of some fundamental properties (firing rate r_0, coefficient of variation $C_{V,0}$, susceptibility χ_0, and firing rate curve f_I) it requires a minimal degree of stationarity that allows to estimate these properties. Another interesting question in this context is how transients in the prescribed statistics, e.g., a slowly changing rate or CV of the prescribed spike train, can be incorporated into our method. One possibility for this could be to use sequences of piecewise constant prescribed statistics. In this case the method could remain unchanged and the change of the spike-train parameters would be achieved by changing the respective parameter from trial to trial.

Turning to applications, we hope that our method opens up new opportunities in experiments. Testing the behavioral response to specific spike patterns, for instance, becomes possible with our method. In particular, the dependence of the effect size of the behavioral response on the irregularity of spike patterns [12] could be studied in a more systematic manner than previously done. Although some experiments are necessary to calculate the susceptibility and the rate-vs-input-current relation, not too much data are needed to estimate these functions. Due to its simplicity, our approach can be a useful tool in reverse-physiology experiments.

[1] S. P. Strong, R. Koberle, R. R. de Ruyter van Steveninck, and W. Bialek, Phys. Rev. Lett. **80**, 197 (1998).

[2] Y. Zuo, H. Safaai, G. Notaro, A. Mazzoni, S. Panzeri, and M. E. Diamond, Curr. Biol. **25**, 357 (2015).

[3] W. R. Softky and C. Koch, J. Neurosci. **13**, 334 (1993).

[4] M. Shadlen and W. Newsome, Curr. Opin. Neurobiol. **4**, 569 (1994).

[5] P. König, A. K. Engel, P. R. Roelfsema, and W. Singer, Neural Comput. **7**, 469 (1995).

[6] M. London, A. Roth, L. Beeren, M. Haeusser, and P. E. Latham, Nature (London) **466**, 123 (2010).

[7] T. Tchumatchenko, A. Malyshev, F. Wolf, and M. Volgushev, J. Neurosci. **31**, 12171 (2011).

[8] S. Deneve and C. K. Machens, Nat. Neurosci. **19**, 375 (2016).

[9] M. Brecht, M. Schneider, B. Sakmann, and T. W. Margrie, Nature (London) **427**, 704 (2004).

[10] A. R. Houweling and M. Brecht, Nature (London) **451**, 65 (2008).

[11] C. T. Li, M. Poo, and Y. Dan, Science **324**, 643 (2009).

[12] G. Doron, M. von Heimendahl, P. Schlattmann, A. R. Houweling, and M. Brecht, Neuron **81**, 653 (2014).

[13] D. Bernardi and B. Lindner, Phys. Rev. Lett. **118**, 268301 (2017).

[14] J. Doose, G. Doron, M. Brecht, and B. Lindner, J. Neurosci. **36**, 11120 (2016).

[15] M. C. Stüttgen, L. J. P. Nonkes, H. R. A. P. Geis, P. H. Tiesinga, and A. R. Houweling, J. Neurophysiol. **117**, 1363 (2017).

[16] P. Lansky and S. Ditlevsen, Biol. Cybern. **99**, 253 (2008).

[17] P. Hänggi and P. Jung, Adv. Chem. Phys. **89**, 239 (1995).

[18] P. M. Harrison, L. Badel, M. J. Wall, and M. J. E. Richardson, PLoS Comput. Biol. **11**, 1004165 (2015).

[19] S. Ostojic, G. Szapiro, E. Schwartz, B. Barbour, N. Brunel, and V. Hakim, J. Neurosci. **35**, 7056 (2015).

[20] N. Fourcaud-Trocmé, D. Hansel, C. van Vreeswijk, and N. Brunel, J. Neurosci. **23**, 11628 (2003).

[21] R. S. L. Gomez, R. Budelli, M. Stiber, and J. P. Segundo, Biol. Cybern. **92**, 110127 (2005).

[22] R. Brette, Neural Comput. **02**, 188 (2009).

[23] J. H. Macke, P. Berens, A. S. Ecker, A. S. Tolias, and M. Bethge, Neural Comput. **21**, 397 (2009).

[24] G. L. Gerstein and B. Mandelbrot, Biophys. J. **4**, 41 (1964).

[25] A. V. Holden, *Models of the Stochastic Activity of Neurones* (Springer-Verlag, Berlin, 1976).

[26] R. D. Vilela and B. Lindner, J. Theor. Biol. **257**, 90 (2009).

[27] J. Nichols, C. Olson, J. Michalowicz, and F. Bucholtz, Prob. Eng. Mech. **25**, 315 (2010).

[28] N. Brunel and S. Sergi, J. Theor. Biol. **195**, 87 (1998).

[29] W. M. Kistler, W. Gerstner, and J. L. van Hemmen, Neural Comput. **9**, 1015 (1997).

[30] R. Jolivet, R. Kobayashi, A. Rauch, R. Naud, S. Shinomoto, and W. Gerstner, J. Neurosci. Meth. **169**, 417 (2008).

[31] R. D. Vilela and B. Lindner, Phys. Rev. E. **80**, 031909 (2009).

[32] C. Bauermeister, T. Schwalger, D. Russell, A. B. Neiman, and B. Lindner, PLoS Comput. Biol. **9**, e1003170 (2013).

[33] T. Schwalger, D. Miklody, and B. Lindner, Eur. Phys. J. Spec. Topics **222**, 2655 (2013).

[34] T. Schwalger, F. Droste, and B. Lindner, J. Comput. Neurosci. **39**, 29 (2015).

[35] R. Moreno-Bote and N. Parga, Neural Comput. **22**, 1528 (2010).

[36] F. Farkhooi, M. F. Strube-Bloss, and M. P. Nawrot, Phys. Rev. E. **79**, 021905 (2009).

[37] M. J. Chacron, K. Pakdaman, and A. Longtin, Neural Comput. **15**, 253 (2003).

[38] M. J. Chacron, B. Lindner, and A. Longtin, Phys. Rev. Lett. **93**, 059904(E) (2004).

[39] W. H. Nesse, L. Maler, and A. Longtin, Proc. Natl. Acad. Sci. USA **107**, 21973 (2010).

[40] B. Doiron, C. Laing, A. Longtin, and L. Maler, J. Comput. Neurosci. **12**, 5 (2002).

[41] E. M. Izhikevich, IEEE Trans. Neur. Net. **15**, 1063 (2004).